Mechanism of zinc oxide retardation in alkali-activated materials: An *in situ* X-ray pair distribution function investigation

Supplementary Information

Nishant Garg[1] and Claire E. White[1*]

[1]*Department of Civil and Environmental Engineering and Andlinger Center for Energy and the Environment, Princeton University, Princeton, USA*

* Corresponding author: Phone: +1 609 258 6263, Fax: +1 609 258 2799, Email: whitece@princeton.edu

Postal address: Department of Civil and Environmental Engineering, Princeton University, Princeton NJ 08544, USA

Isothermal Calorimetry of Alkali-activated Slag

According to the literature, the heat evolution in an AAS is directly dependent on the type of the activator used.[1,2] For the case of a sodium silicate-based activator, similar to what is used here, a standard reaction pathway of pre-induction period, induction period, acceleration, and deceleration has been reported.[3] The induction period refers to a period of little to no activity and is very similar to the one commonly observed in the hydration of OPC-based binders.[4]

Peak Assignments for X-ray PDF of Alkali-activated Slag

The peak in the vicinity of 1.64 Å is assigned to the T-O bond length, based upon the reported Si-O bond distance of ~1.60 Å and the Al-O bond distance of ~1.75 Å when Si/Al are present as tetrahedral units in disordered calcium aluminosilicates.[5,6] It should be noted that aluminum is primarily present as a tetrahedral unit in slag as confirmed by PDF,[7] nuclear magnetic resonance,[8] and molecular dynamics simulations.[9] The peak at ~2.31 Å is assigned to the Ca-O nearest-neighbor correlation based on previous studies on glasses,[6,10] while the peak at ~3.10 Å is assigned to T-T correlations as all Si-Al, Al-Al, and Si-Si correlations have been reported to coincide around this region.[11] Finally, the peak at ~3.60 Å is assigned to Ca-T correlations based on a C-S-H model proposed in the literature.[12]

Isothermal Calorimetry of Alkali-activated Metakaolin

The differences between the reaction kinetics of AAS and AAM pastes are expected because of the vastly different precursor chemistries together with differences in the concentration of the activators. The precursor in AAS paste is slag which is an amorphous calcium aluminosilicate (with some magnesium),[7] whereas the precursor in AAM paste is dehydroxylated kaolinite, or metakaolin, which is an amorphous aluminosilicate. The activator in AAS has a Na_2O/slag wt. ratio of 0.04, whereas the activator in AAM is much more concentrated with a 0.28 wt. ratio for Na_2O/metakaolin. The higher sodium concentration for the metakaolin pastes is required to invoke a significant amount of dissolution during the initial stages of reaction and to ensure proper charge-balancing of the negative tetrahedral alumina sites in the resulting N-A-S-(H) gel. Due to the weakly cementitious properties of slag together with the abundance of calcium in the precursor

(and lower concentration of aluminum compared with metakaolin), a much lower sodium concentration can be used in the activator. Thus, it is not surprising that the heat evolution kinetics of these pastes are vastly different.

The heat evolution curves shown in Figure 4 in the Article are in general agreement with what has been reported in the literature for metakaolin activated with sodium hydroxide[13] and sodium silicate.[14] In these studies, three peaks were identified, including a sharp first peak which corresponds to the dissolution of the aluminosilicate, a second broad peak which signifies the major reaction and formation of the N-A-S-(H) gel, and a third small peak at a later stage which is seen when/if the N-A-S-(H) gel becomes more ordered (which is more common for the hydroxide-activated metakaolin pastes). In the data reported here, the early sharp peak associated with dissolution was probably located within the first hour of data (not included in Figure 4 in the Article), but remnants of it can be seen in Figure 4 in the Article at the 1 hr reaction time mark. The second broad peak, corresponding to the formation of the main reaction product, is clearly visible between ~ 1 and 30 hrs. Finally, the third peak is not present in the data, suggesting that the gel remains predominantly amorphous throughout the reaction period.

Peak Assignments for X-ray PDF of Alkali-activated Metakaolin

The peak assignments of the nearest-neighbor T-O and T-T correlations have been carried out in a similar fashion to what was described earlier for AAS. Apart from these correlations, there are three additional major atom-atom correlations in Figure 5 in the Article, i.e., Na-O at ~2.30 Å, O-O at ~2.60 Å, and T-Na at ~3.15 Å. These assignments are based on the simulated PDFs of

hydrosodalite ($Na_6(AlSiO_4)_6(H_2O)_8$),[15] which possesses a stoichiometry and network structure similar to the AAM system studied here.[11]

Evolution of the CZ Phase

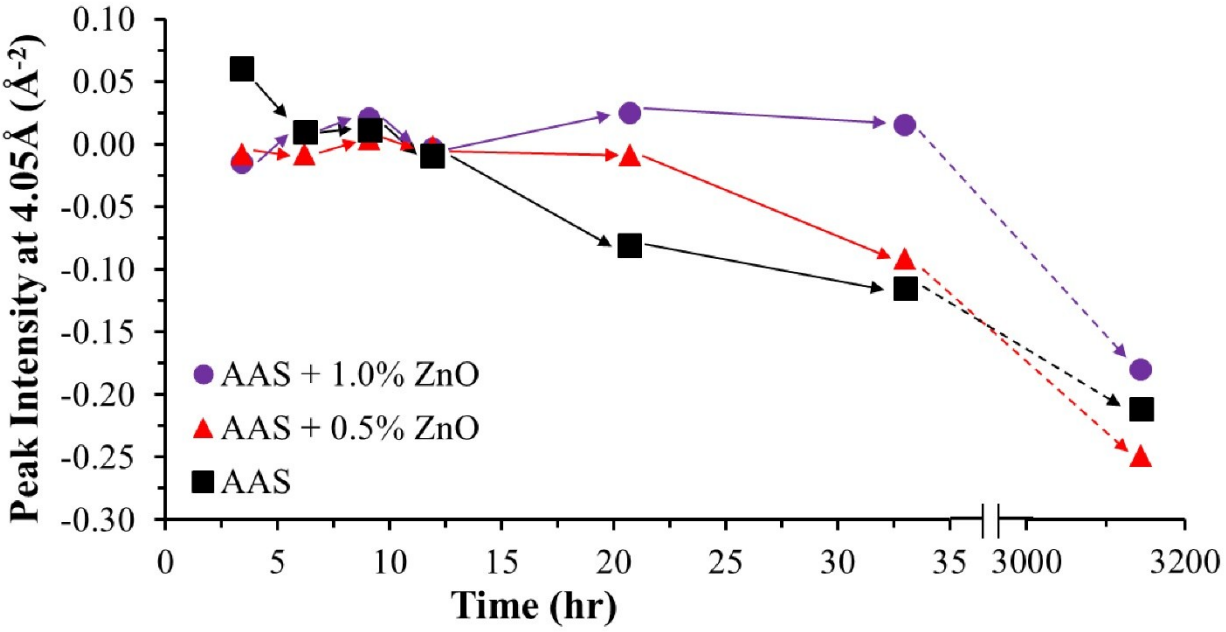

Figure S1: The intensity at 4.05 Å in the difference curves plotted in Figure 8 in the Article as a function of the alkali-activation reaction for the AAS paste samples. Also, the arrows for selected pastes are plotted to guide the eye.

Evolution of the Diffraction Patterns of Alkali-activated Slag with and without Nano-ZnO

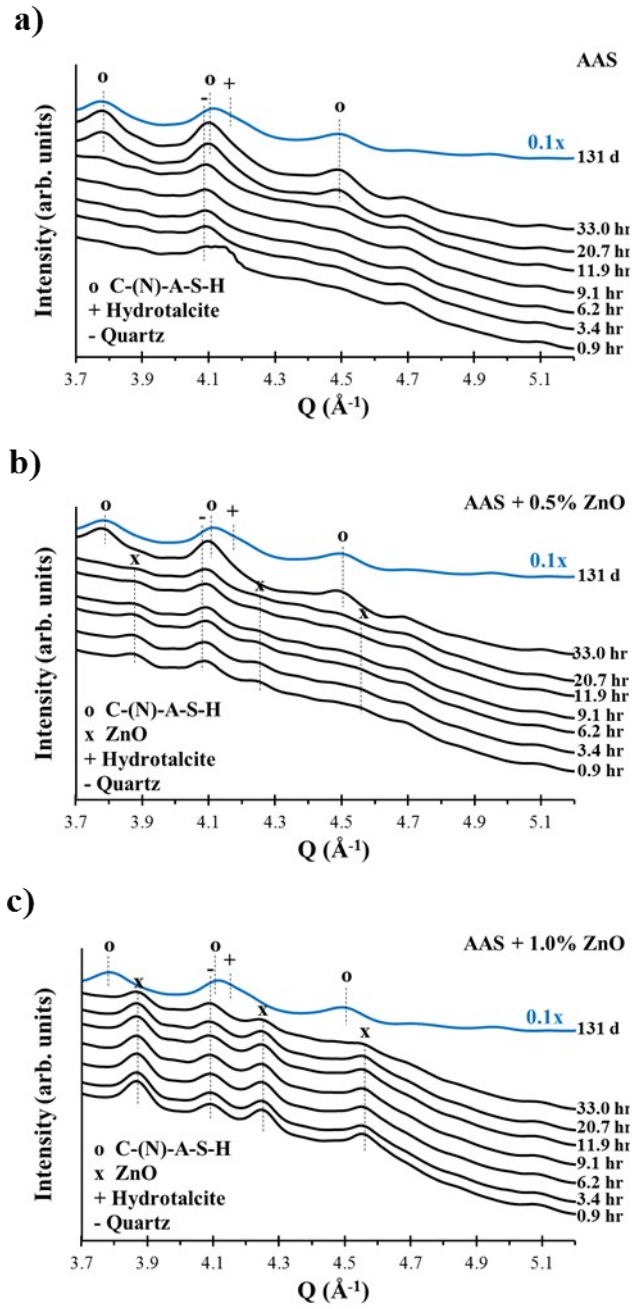

Figure S2: Stacked plots of the X-ray diffraction patterns of AAS paste with and without nano-ZnO at the given reaction times. The peaks from the C-(N)-A-S-H gel phase, hydrotalcite, quartz, and zinc oxide (hexagonal crystal structure) are identified. The patterns at 131 day have been scaled by a factor of 0.1 owing to their high intensity.

Peak assignments in Figure S2 were carried out as follows: C-(N)-A-S-H gel (disordered C-S-H (I), PDF #00-034-0002), hydrotalcite ($Mg_6Al_2CO_3(OH)_{16}\cdot 4(H_2O)$, PDF #00-034-0002), quartz (SiO_2, PDF #00-005-0490), and zinc oxide (ZnO, PDF #00-036-1451). Since the peak at ~4.09 $Å^{-1}$ is present in all samples throughout the reaction, it is likely to be a crystalline impurity in the precursor slag (i.e., quartz).[16]

References

1 Z. Huanhai, W. Xuequan, X. Zhongzi and T. Mingshu, *Cem. Concr. Res.*, 1993, **23**, 1253–1258.

2 A. Fernández-Jiménez and F. Puertas, *Cem. Concr. Res.*, 1997, **27**, 359–368.

3 C. Shi and R. L. Day, *Cem. Concr. Res.*, 1995, **25**, 1333–1346.

4 J. W. Bullard, H. M. Jennings, R. A. Livingston, A. Nonat, G. W. Scherer, J. S. Schweitzer, K. L. Scrivener and J. J. Thomas, *Cem. Concr. Res.*, 2011, **41**, 1208–1223.

5 J. B. Jones, *Acta Crystallogr. Sect. B.*, 1968, **24**, 355–358.

6 V. Petkov, S. J. L. Billinge, S. D. Shastri and B. Himmel, *Phys. Rev. Lett.*, 2000, **85**, 3436-3439.

7 K. Gong and C. E. White, *Cem. Concr. Res.*, 2016, **89**, 310–319.

8 K. Shimoda, Y. Tobu, K. Kanehashi, T. Nemoto and K. Saito, *J. Non-Cryst. Solids*, 2008, **354**, 1036–1043.

9 K. Shimoda and K. Saito, *ISIJ Int.*, 2007, **47**, 1275–1279.

10 L. Cormier, D. Ghaleb, D. R. Neuville, J.-M. Delaye and G. Calas, *J. Non-Cryst. Solids*, 2003, **332**, 255–270.

11 C. E. White, K. Page, N. J. Henson and J. L. Provis, *Appl. Clay Sci.*, 2013, **73**, 17–25.

12 R. J.-M. Pellenq, A. Kushima, R. Shahsavari, K. J. Van Vliet, M. J. Buehler, S. Yip and F.-J. Ulm, *Proc. Natl. Acad. Sci. U. S. A.*, 2009, **106**, 16102–7.

13 Z. Zhang, H. Wang, J. L. Provis, F. Bullen, A. Reid and Y. Zhu, *Thermochim. Acta*, 2012, **539**, 23–33.

14 Z. Zhang, J. L. Provis, H. Wang, F. Bullen and A. Reid, *Thermochim. Acta*, 2013, **565**, 163–171.

15 M. M. Murshed and T. M. Gesing, *Zeitschrift für Krist.*, 2008, **223**, 178–185.

16 A. E. Morandeau and C. E. White, *Chem. Mater.*, 2015, **27**, 6625–6634.